Computers and Geotechnics 141 (2022) 104547

Contents lists available at ScienceDirect

Computers and Geotechnics

journal homepage: www.elsevier.com/locate/compgeo

Experimental validation of a simplified numerical model to predict train-induced ground vibrations

Abdul Ahad Faizan [a], Osman Kırtel [a,*], Erkan Çelebi [b], Abdullah Can Zülfikar [c], Fatih Göktepe [d]

[a] Sakarya University of Applied Sciences, 54187 Esentepe Campus, Sakarya, Turkey
[b] Sakarya University, 54187 Esentepe Campus, Sakarya, Turkey
[c] Gebze Technical University, 41400 Cayirova Campus, Kocaeli, Turkey
[d] Bartın University, 74100 Kutlubey-Yazıcılar Campus, Bartın, Turkey

ARTICLE INFO

Keywords:
High-speed train
Free-field motion
Finite element method
Absorbing boundary
2D numerical model
Experimental verification

ABSTRACT

This study evaluates the effect of high-speed train (HST)-induced environmental vibrations using simplified computational models and validates the test results in full-scale field conditions. Experimental investigations and in-situ measurements were performed at the Istanbul-Ankara high-speed railway section to examine the effect of ground vibrations from HSTs on the surrounding residential lands. In this study, ground-borne free-field surface motion at different distances from the railway track was realized using accelerometers. The experimental results of vertical and horizontal ground vibration accelerations induced by HSTs with a velocity of 250 km/h were analyzed. In the first part of the study, a two-dimensional (2D) numerical model based on finite element method (FEM) was used to investigate ground vibrations and validate the experimental results. To minimize artificial reflections and dissipate vibrational energy at the boundaries, the lateral extension of an infinite domain was modeled with viscous absorbing boundaries. A dynamic analysis of the proposed railway-soil coupled model was performed in the time domain under plain-strain conditions using Plaxis 2D, a commercial FEM software. For the verification, the experimental results were compared with those obtained from the numerical analysis. The simplified computational model validated by the test results may help researchers determine further investigation strategies to develop cost-effective mitigation measures for structures with sensitive devices near the railway track and significantly contribute to understanding complex wave propagation problems. In the second part of the study, train-induced environmental ground vibrations were analyzed for different types of soil conditions using a 2D FE model. Computational analyses were performed with four types of soil: soft, medium, dense, and rock, based on the Turkish Earthquake Code. The HST was used as a dynamic source to observe the differences in vibration generation and wave transmission in different types of soil. The HST load on the slab track was simulated to study the effect of operational loads on ground-borne vibrations. Based on the dynamic analysis results, the response of the free-field motion was investigated to obtain the relative acceleration time histories for different points of soil. According to the results, the peak acceleration values of train-induced vibrations at soft, medium, and dense soil sites increased dramatically when compared to the rock site. Vibration measurement data collected from parametric experiments with a simple numerical model for various soil characteristics can be particularly useful when planning residential and industrial facilities at new locations near railroads, to avoid the adverse effects of environmental vibrations caused by HSTs.

1. Introduction

With the recent economic development, railway networks for high-speed trains (HSTs) have grown in several countries. For instance, the Turkish State Railways (TCDD) launched the construction of a high-speed railway network in the country in 2003. Since then, 1.213 km high-speed lines have been constructed and put into operation for trains running at a speed of 250–300 km/h. With the completion of these projects, the total length of railways in Turkey is expected to reach 25,000 km by 2023 (TCDD, 2017). YHT is the only high-speed rail service in Turkey with two types of trains operating at speeds of up to 250–300 km/h and a maximum axle load of 225 kN.

* Corresponding author.
E-mail address: okirtel@subu.edu.tr (O. Kırtel).

https://doi.org/10.1016/j.compgeo.2021.104547
Received 11 March 2021; Received in revised form 2 November 2021; Accepted 4 November 2021
Available online 16 November 2021

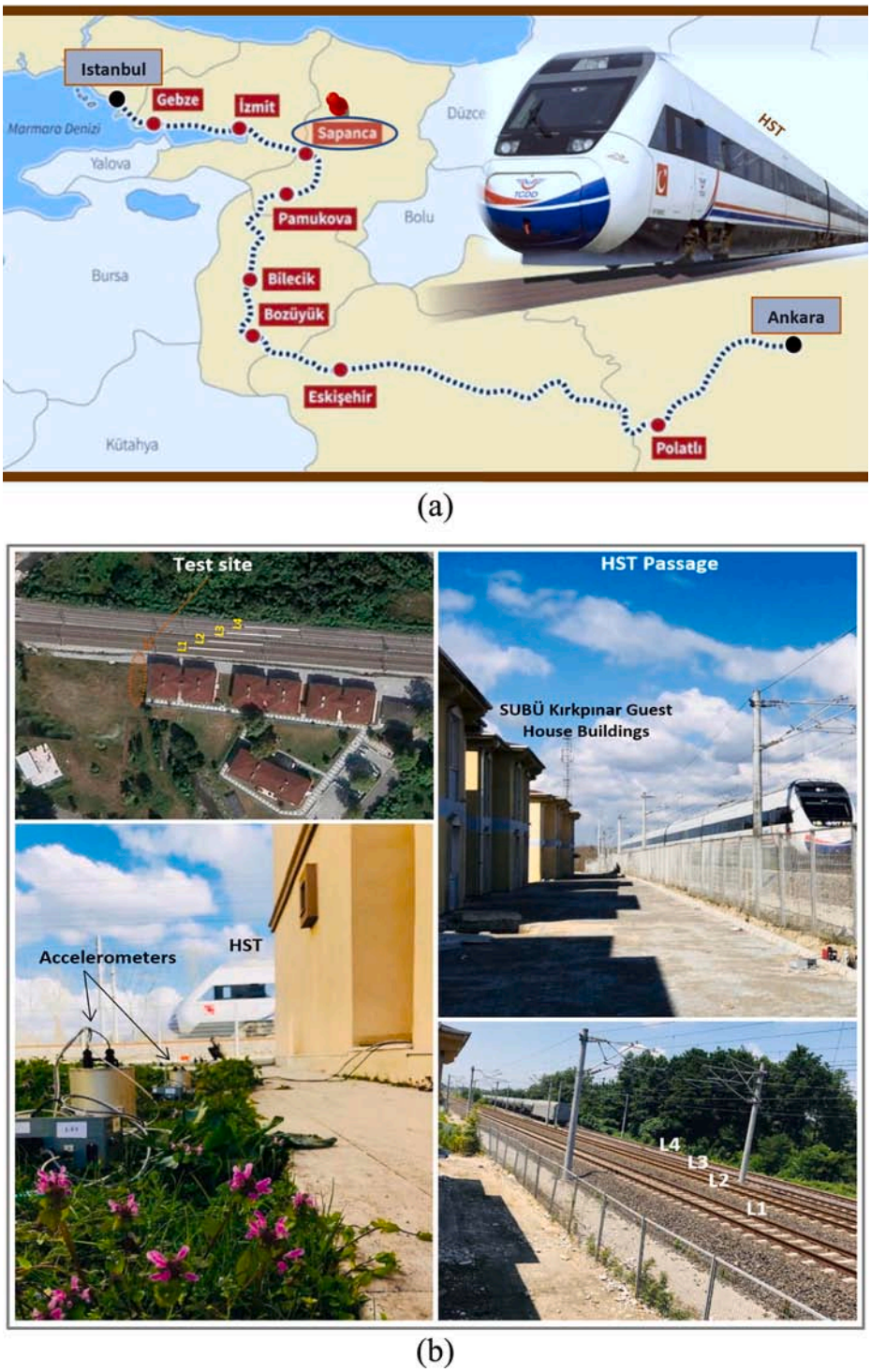

Fig. 1. (a) Location of the railway and (b) details of the measurement site.

With the rapid increase and development of HSTs, problems such as train-induced vibration and its dynamic effects on nearby structures have become a major environmental concern in urban areas. Ground-borne vibrations from HSTs pose a challenge for field engineers building structures in residential areas. The effect of vibrations from traffic systems on urban life and working environment has been brought to public attention because vibration is listed as one of the seven major environmental hazards worldwide (Gupta et al., 2009). Therefore, a thorough analysis of these effects is necessary to avoid possible problems to buildings that may be exposed to train-induced vibrations. There has been a considerable amount of research on train-induced vibrations in the recent years. These studies can be categorized into field measurements, experimental tests, and numerical studies.

Several studies have used analytical and numerical modeling to investigate train-induced vibrations (Auersch, 1994; Sheng et al., 1999; Metrikine and Vrouwenvelder, 2000; Liao et al., 2005; Forrest and Hunt, 2006; Wanming et al., 2010). Triepaischajonsak and Thompson (2015) used a hybrid approach to study train-induced ground vibrations by considering the train-track interaction. Yang et al. (2003) developed a model to study wave propagation in layered soils induced by different

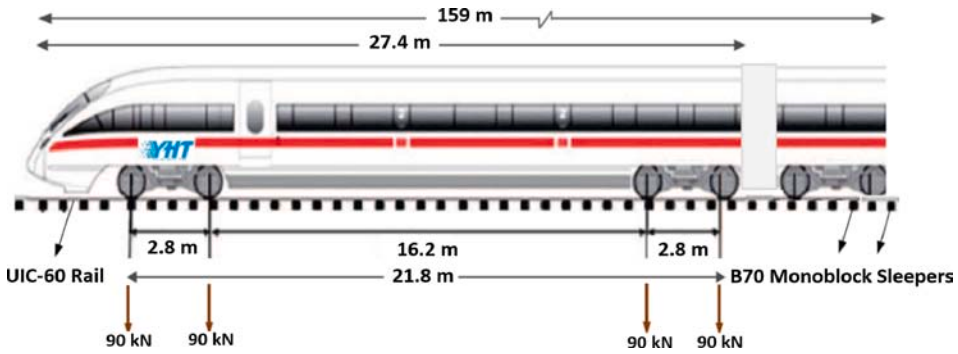

Fig. 2. Geometrical characteristics and axle load of train HT65000.

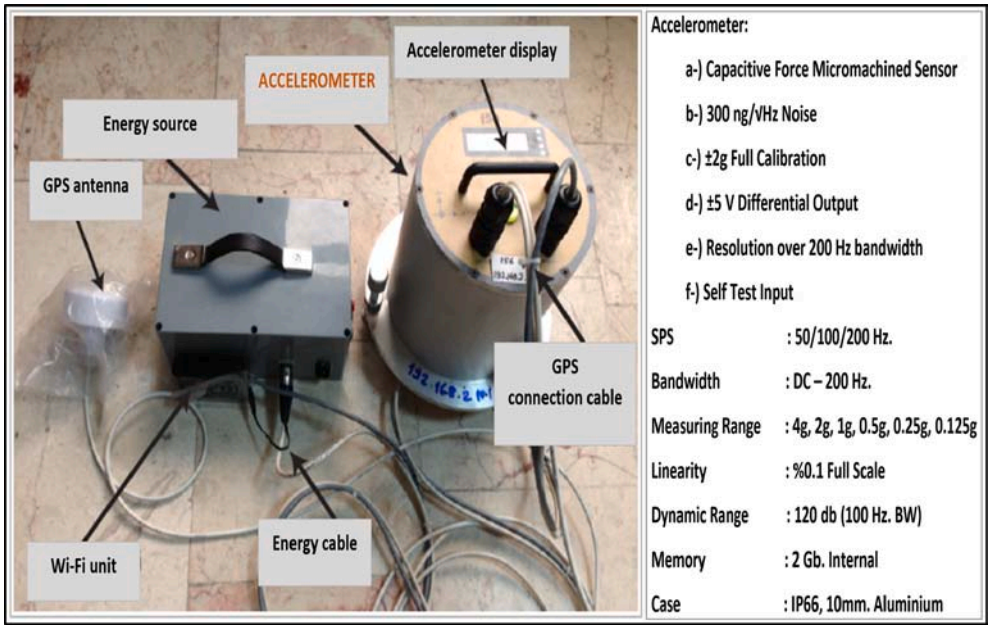

Fig. 3. Accelerometer properties.

train speeds. Lombaert and Degrande (2009) suggested a numerical model to investigate the quasi-static and dynamic excitations from train-induced ground vibrations. Gupta et al. (2008) studied Beijing's subway Line 4 train vibrations using a combined finite element method (FEM)/boundary element method (BEM method). In numerical modeling, FEM (Takemiya, 2003; Celebi, 2006; Connolly et al., 2013; Kouroussis and Verlinden, 2013), BEM (François et al., 2005; Galvín et al., 2010), and combined methods (Sheng et al., 2005; Andersen and Jones, 2006; Costa et al., 2012; Yaseri et al., 2014; Galvín and Romero, 2014) have been used to study train-induced vibrations. Zou et al. (2020) presented a prediction method for building vibration and structure-radiated noise caused by train-induced vibration. Studies on the effect of soil conditions have proposed ground improvement to mitigate vibration and structure-radiated noise within buildings. Thompson et al. (2016) employed a 2.5D FE/BE method to reduce the effect of train-induced ground-borne vibrations using open trenches and soft-filled barriers. Kontoni and Farghaly (2020) developed a three-dimensional (3D) finite element (FE) model to investigate the effect of train-induced ground vibrations near high-rise buildings. Different vibration mitigation trench techniques, such as open or geofoam-filled trenches, were analyzed to determine the most suitable technique for mitigating the effect of induced vibrations. Chen et al. (2021) proposed a new method for isolating ground vibrations using horizontally buried hollow pipes. These pipes reduced the effect of ground-borne vibrations because of harmonic stress excitation and their performance was investigated using an FE model under plain-strain conditions.

In addition to the above-mentioned analytical and numerical methods, several experimental studies have evaluated train-induced ground vibrations. To overcome some of the limitations associated with numerical analysis methods, researchers have performed several in-situ measurements on various railway sites to investigate the practical vibration propagation characteristics (Degrande and Schillemans 2001; Kogut et al., 2003; Galvín & Domínguez, 2009). Xia et al. (2009) performed a series of in-situ experiments to study the effect of train-induced vibrations on the ground and nearby structures. Zhang and Feng (2011) studied the characteristics of high-speed train-induced ground vibrations in the Hu-Ning Railway using an experimental method. Degrande and Schillemans (2001) measured train-induced ground vibration near the Brussels-Paris HSR line with train speeds between 223 and 314 km/h to validate a numerical model. Çelebi et al. (2009) performed a series of in-situ experiments to study the effect of open- or in-filled trench barriers as a reduction measure for soil vibrations from a moving load, which is considered a stationary wave source. Auersch (2005) performed a series of ground vibration measurements during the test runs of an ICE train at various speeds near Würzburg. In addition, many field measurements have been performed and validated by comparing the numerical and experimental results of predicted train-induced vibrations (Lombaert and Degrande 2001; Lombaert et al., 2006; Gupta et al.,

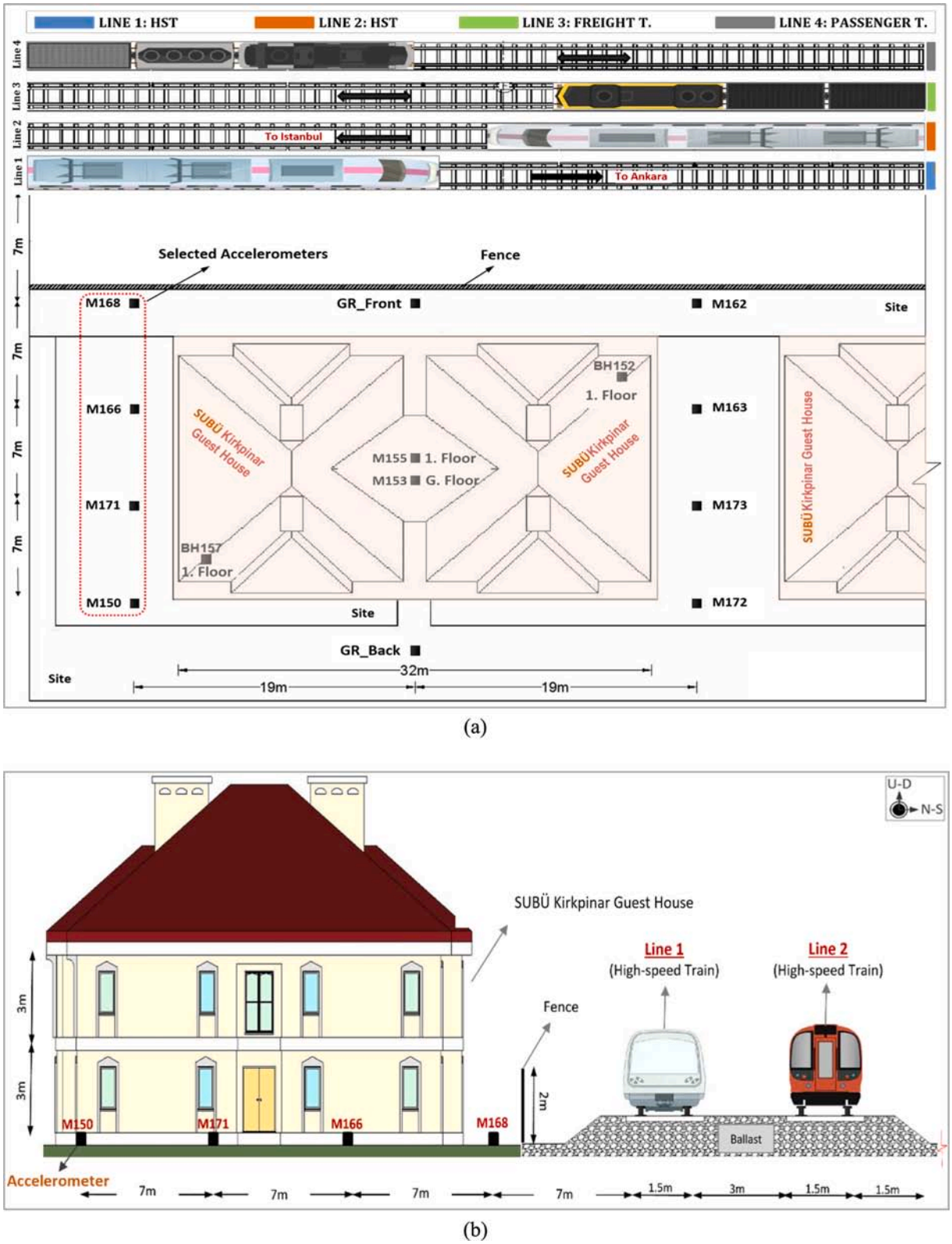

Fig. 4. Schematic diagrams of measuring point arrangement (a) top view and (b) cross-section view.

2008).

Calculation time is a key point in the simulation of an FE model. 3D FE modeling essentially requires larger computational times than two-dimensional (2D) modeling. The biggest advantage of 2D modeling is its simplicity — it requires less computational time and enables researchers to easily amend a project and perform an analysis with a small file size, thereby saving time. Therefore, simplifying complex 3D models into 2D for shorter computational times and a faster analysis is desirable for sensitivity and optimization. Andersen and Jones (2006) performed 2D and 3D FE analyses and observed that the results of 2D models qualitatively agree with those of the 3D models at most frequencies, which explains the preference for 2D models. Therefore, this study

Fig. 5. Passage of the HT65000 high-speed train on Line 1 with speed V = 250 km/h (Kirkpinar, Sakarya 2018).

selected a 2D FE model to achieve consistent results.

This study focuses on two aspects. First, the authors performed in-situ measurements and ground-borne vibration experiments on the Istanbul-Ankara HSR. The speed of the test train was 250 km/h. Then, a 2D numerical model based on FEM was used to study ground-borne vibrations and validate the experimental results. Based on the obtained results, we conclude that the simulated numerical model can replicate the experimental data and be applied to analyze vibrations. Subsequently, this verified model was used to study the influence of train-induced vibrations on different soil conditions. Four types of soil (soft, medium, dense, and rock) were used to this end. Finally, the computed results are discussed to arrive at some useful conclusions.

2. Characteristics of the train and test site

In July 2018, a free-field measurement on the Istanbul-Ankara HSR, with a total length of 533 km, was performed at a train speed of 250 km/h. The measurement was performed at Kirkpinar in Sakarya, where the SUBÜ Kirkpinar Guest House is located. The proposed test location was near the Arifiye train station. The HSR line passes through the Kirkpinar village, which is located at the western end of the Sapanca district. This location was chosen because of its weak soil condition ($V_S = 200$ m/s), proximity to the train line, and distance from any vibration generating environments. There are four railway lines near the buildings. These buildings are located 8–10 m away from Line 1, as shown in Fig. 1. These measurements were conducted to determine the free-field ground motion produced by repeated train passages. These field measurement results were subsequently used to validate the numerical prediction model. Line L1, which stretches from Istanbul to Ankara, was selected for this purpose.

TCDD HT65000 is considered as the test train. It consists of six cars but can be reconstructed as an eight-car unit depending on the number of passengers. Each axle has a set of right and left wheels and the axle load of the car is 180 kN. The distance between the first and last axles is 21.8 m, which, in terms of time, takes 0.314 sec with a speed of 250 km/h. The distance between the wheels is 2.8 m. This train is approximately 159 m long, with a passenger capacity of 419. The train moves over a ballasted track consisting of UIC-60 rails and B70 monoblock sleepers. The train characteristics are shown in Fig. 2.

Table 1
Overview of recorded high-speed train passages.

Track	Direction	Passage	Date and time 17–07-2018			
1	Istanbul - Ankara	4	09:40	11:04	12:15	13:34

3. In-situ experiments and measurements

3.1. Vibration test instruments

This study used DAC-3HDG accelerometers for the field tests. DAC-3HDG has a high accuracy and linearity, 32-bit ADC, 120 dB (100 Hz BW) dynamic range, and an extremely low noise level. This 3-axis capacitive force micromachined sensor is capable of measuring and monitoring strong-motion seismic activity and low-level ambient vibrations. The accelerometer has a plug-and-play design that includes a Wi-Fi/power unit and a global positioning system (GPS) antenna to measure the vibrations radiated from a train to its environment. The devices used in the field measurements consist of three basic parts: a GPS antenna, an energy source, and an accelerometer main box. The technical properties of these devices are summarized in Fig. 3.

3.2. Measuring point arrangement

Fig. 4 shows the testing instrumentation plan and cross-section for the field measurements performed in July 2018 at Kirkpinar, Sakarya. There are four railway lines at the testing site. The ground-borne vibrations were recorded at this site for a variety of train passages, including passenger trains, freight trains, and high-speed HT65000 trains. On lines L1 and L2, HSTs connecting Istanbul with Ankara operate, while lines L3 and L4 are used for freight transportation and suburban passenger traffic purposes. Measurements were performed at 14 points in three directions during the passage of the trains. The directions are defined as N-S (perpendicular to the track), E-W (parallel to the track), and U-D (vertical downward). In total, 14 accelerometers were placed perpendicular to the railway track to record the train vibrations. Ten accelerometers were located on the ground surface, and the other four were placed in the building. The passage of trains on all tracks was recorded during the measurements. This study considered the data from four measurements (M168, M166, M171, and M150) during the passage of HST at 09:40 AM to validate the numerical prediction model. These accelerometers were placed at distances of 7, 14, 21, and 28 m from Line 1 (see Fig. 4).

3.3. Recorded passages

Four train passages were recorded by M168, M166, M171, and M150 accelerometers to observe the ground vibration. These measurements were performed during passages of the HSTs on line L1 at a speed of 250 km/h (Fig. 5). The recorded HST passages are presented in Table 1.

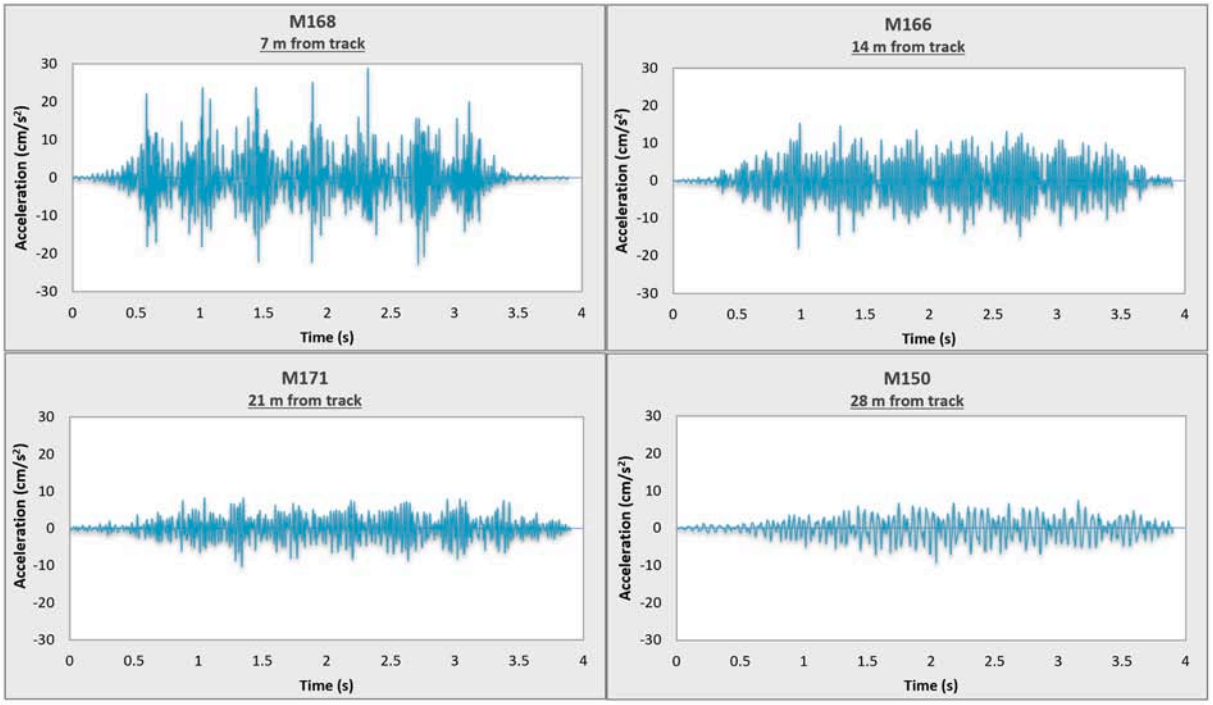

(a)

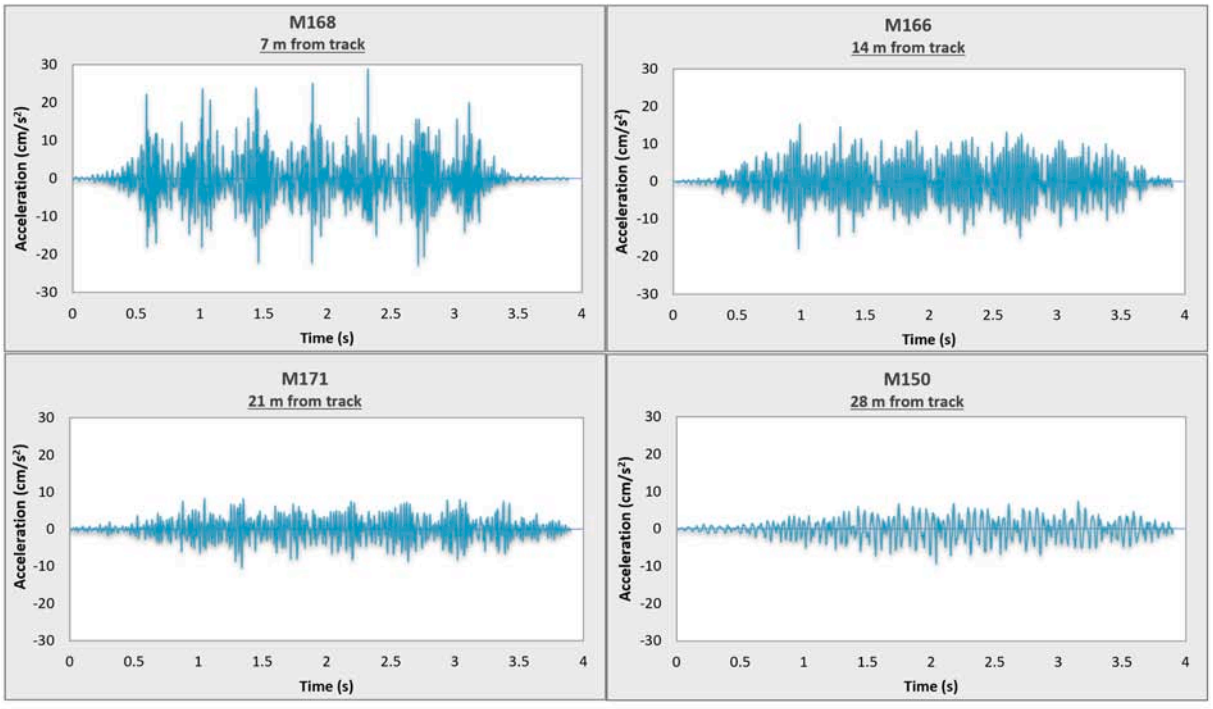

(b)

Fig. 6. Time-histories of the ground vibration accelerations at 7 m, 14 m, 21 m and 28 m from track during the passage of the HT65000 high-speed train on track 1 with speed of 250 km/h. (a) in perpendicular direction and (b) in vertical downward direction.

Table 2
Summary of PGA values for perpendicular and vertical directions.

Device No	Distance from track (m)	a_{N-S} (cm/s^2)	a_{U-D} (cm/s^2)
M168	7	23.00	30.70
M166	14	7.80	12.80
M171	21	8.20	10.20
M150	28	4.30	3.10

3.4. Field measurement results

In this study, the ground vibration during the passage of an HST was recorded in terms of acceleration. The SeismoSignal program was used for converting the raw data into an interpretable form. The measured raw data were baseline-corrected, and a fourth-order Butterworth bandpass filter was applied to them. The frequency range was between 10 Hz and 100 Hz. A time-history analysis was performed in both N-S (perpendicular) and U-D (vertical) directions to extract the peak ground accelerations (PGAs). Fig. 6 summarizes the time histories of the vertical and parallel accelerations at all distances from track 1. The extracted PGAs are presented in Table 2.

Fig. 6 and Table 2 show that the vibration levels generally tend to decrease with distance from the track. In the perpendicular direction, the PGA for M168 is equal to 23 cm/s^2 at x = 7 m from the track and the PGA for M150 is equal to 4.3 cm/s^2 at x = 28 m from the track. When considering the results in the vertical direction, the PGA for M168 is equal to 30.7 cm/s^2 at x = 7 m, and the PGA for M150 is equal to 3.1 cm/s^2 at x = 28 m. Moreover, the PGA results for both directions show that train vibrations have more impact in the downward (U-D) direction than in the perpendicular (N-S) direction.

4. Numerical prediction model

4.1. Discretization of FE model

For the model's numerical computations with the simulated train load, 2D FE analyses with the Plaxis software package (Brinkgreve et al., 2002) were utilized in the time domain for an extensive parametric study. In a dynamic analysis, the model dimensions and boundaries must be carefully selected to improve accuracy and reduce computational effort (Galavi and Brinkgreve 2014; Çelebi and Kırtel 2013; Faizan and Kırtel 2017). The discretization size of the conceded numerical model should be carefully selected to avoid boundary effects (Kumar et al., 2017; Kumar & Choudhury, 2018). Several analyses have been performed in the past to determine the dimensions of a suitable FE model. These boundary areas must be at least 8–10 times and 4–5 times the superstructure base width and soil depth, respectively (Rosset and Kausel 1976; Faizan, 2017). This study's H and L values were determined using these criteria.

It is known that the formation of excess pore water pressure is strongly affected by an increase in both the amplitude and frequency of cyclic loading. The influence of cyclic loading on transport corridors, such as highways and railways, has been tested on stone column-reinforced soft soil by Basack et al. (2016). In this study, many important behavioral aspects of stone column–reinforced soft clay under both static and cyclic loadings using the modified cam clay (MCC) model were captured through experimental and numerical investigations. As can be clearly seen from the study results, an increase in both the amplitude and the frequency of cyclic loading has an accelerating effect on the generation of excess pore water pressure. The test medium is composed of soft alluvial soil with a low shear velocity. According to the available data, the geological unit of the region is mainly composed of quaternary-aged deep alluvial deposits. The water table of the case study site is generally high, and it may come closer to the ground surface during the rainy season (Komazawa et al., 2002). The measurement results in the summer and winter seasons show that the PGA values did not change under the same conditions because of the soil's saturated state. Therefore, we determined that the undrained stress–strain response of soft alluvial soil is independent of confining pressure; the reason for this is the changes in pore water pressure because of the saturated state of the soil during a high-speed transition loading. Hence, the groundwater level was not considered in the numerical analysis.

In addition to the existing information, 2D plane-strain analyses of soil were used to determine the appropriate soil dimensions. The response measurement points in the model are the free-soil surfaces, which are named as A, B, and C, respectively, as shown in Fig. 7.

The time histories of the horizontal and vertical vibrations at different measurement points were obtained. First, the effect of wave propagation on the vertical expansion (H) of the soil model was investigated. In each computational model, different values of H, from 10 to 75 m were considered while keeping the total soil length, L, constant at 120 m. After determining the optimal depth of the FE model, the wave propagation effect on the length of the soil model was investigated. Based on the analysis, the displacement–time curves for different soil depths and lengths are given in Fig. 8 and Fig. 9, respectively. A soil

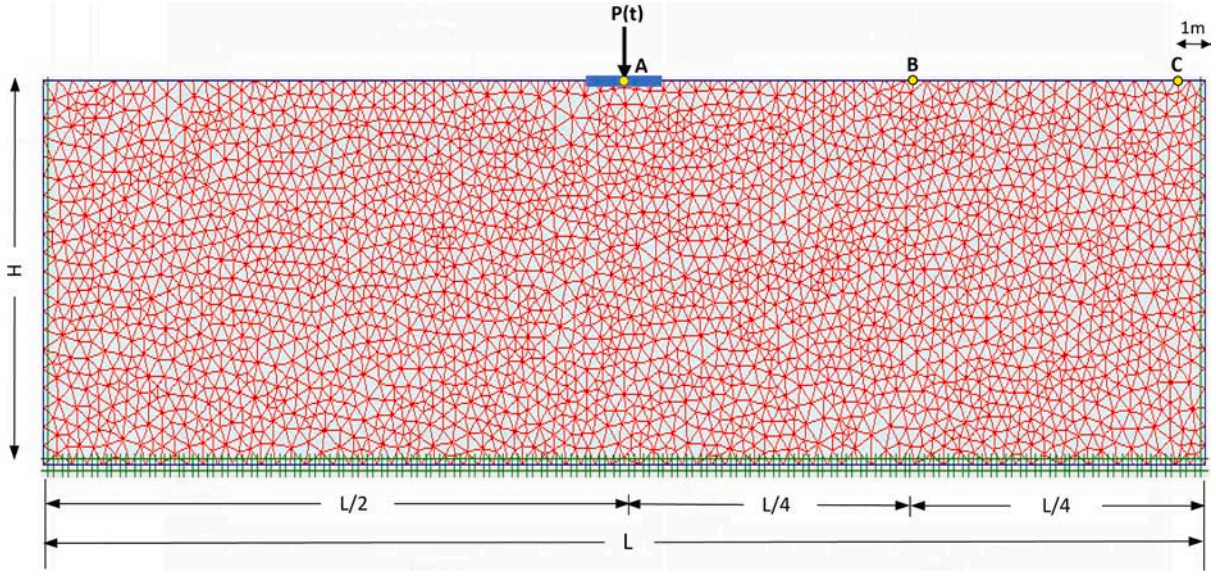

Fig. 7. 2D Numerical model.

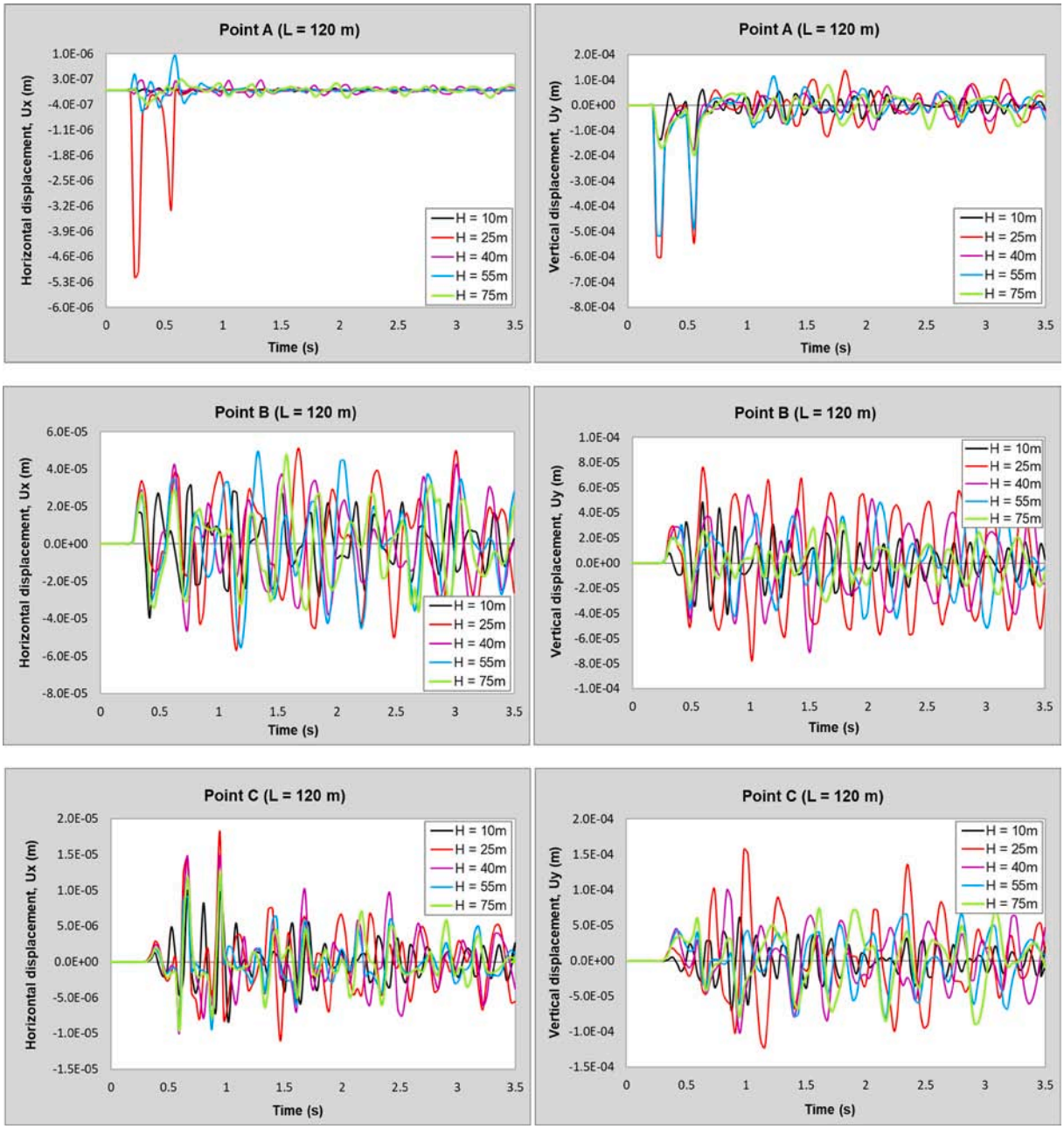

Fig. 8. Determination of the FE model vertical length (depth).

length of L = 160 m and a total depth of H = 40 m were determined to be the optimal sizes for the computations in this study.

One of the major challenges in the dynamic analysis of an FE model of high-speed train-railway-soil interaction problems is achieving a balance between accuracy and economic modeling of soil infinity. To determine the optimum size of the FE soil model, maximum displacement values for different soil widths (L) and depths (H) were obtained at the observation points by performing a dynamic analysis (Fig. 10). By examining the effect of finite soil medium depth (H) on wave propagation (Fig. 10(a)), we observe a convergence of the maximum values of both vertical and horizontal displacements at depths of 40 m and beyond. This convergence is particularly evident in the horizontal displacements. Based on the obtained results, we chose 40 m as the discretized soil depth for the economic modeling.

Fig. 10(b) shows the approximate displacement amplitudes at widths of 160 m and beyond; similar results are observed at the selected points. Based on the results, choosing the height of the soil region as H = 40 m and the length of the soil as L = 160 m can satisfy both the literature criteria and the parametric analysis results.

4.2. FE mesh sensitivity

In this study, a 2D plane-strain FE model was developed in Plaxis 2D using 15-node triangular elements. Each node of these elements have two translational degrees of freedom under plain-strain conditions. Considering the Courant condition for FE model simulations, the FE size (Δh) and time step integration (Δt) were chosen to be 0.75 m and 0.0124 s, respectively. The FE model element size was estimated according to the smallest wavelength, allowing the high-frequency motion to be simulated accurately. The relevant properties of soil were as follows: density, $\gamma = 16.18$ kN/m^3; modulus of elasticity, $E = 1.38 \times 10^5$ kN/m^2; shear wave velocity, $V_S = 170$ m/s; and Poisson's ratio, $\nu = 0.478$.

In an FE analysis, an absorbing boundary must be provided in Plaxis

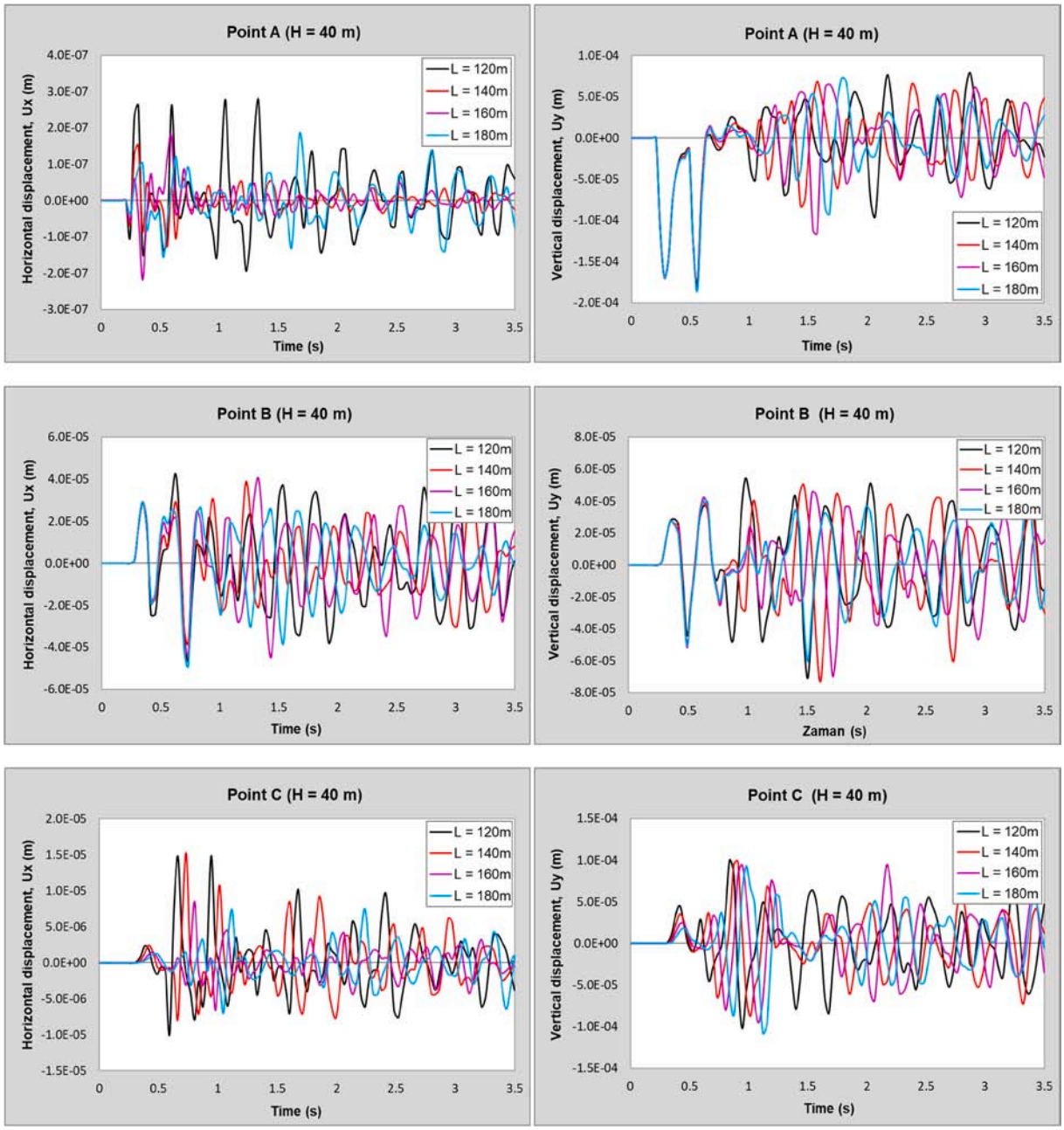

Fig. 9. Determination of the FE model horizontal length.

to absorb stress increments and avoid spurious wave reflections at the model boundaries caused by dynamic loading, which would otherwise be reflected inside the soil body. Therefore, boundary modeling is one of the key points in an FE analysis, and it is necessary to introduce an artificial boundary. In this study, standard fixities and absorbing boundaries were assigned to reduce the wave reflections at the boundaries. The horizontal and vertical sides were fully restrained ($u_x = u_y = 0$). Standard absorbing boundaries were generated at the bottom of the model, the boundary of X_{max} and Ymax, to ensure the stress wave is absorbed. The absorbing boundary used by Plaxis for dynamic analysis is based on the viscous boundary proposed by Lysmer and Kuhlemeyer (1969). The idea is to absorb the stress increments and avoid the wave reflections at model boundaries caused by dynamic loads according to the following equations:

$$\sigma_n = -\rho v_p \frac{\partial_u}{\partial_t} + \sigma_n^0 \tag{1}$$

$$\tau = -\rho v_s \frac{\partial_v}{\partial_t} + \tau^0 \tag{2}$$

where σ_n^0 and τ^0 are the normal and tangential static stresses at the boundary of the main domain, respectively. u and v are the normal and tangential displacements, respectively. The FE model developed in this study is shown in Fig. 11.

The damping in Plaxis is based on hysteretic damping. Rayleigh damping matrix [C] can be represented as a combination of mass matrix [M] and the stiffness matrix [K]. The equation for Rayleigh damping is as follows:

$$[C] = a[M] + \beta[K] \tag{3}$$

where α and β represent the mass- and stiffness-proportional damping coefficients, respectively. Rayleigh α determines the influence of mass on system damping. Rayleigh β is a parameter that determines the effect

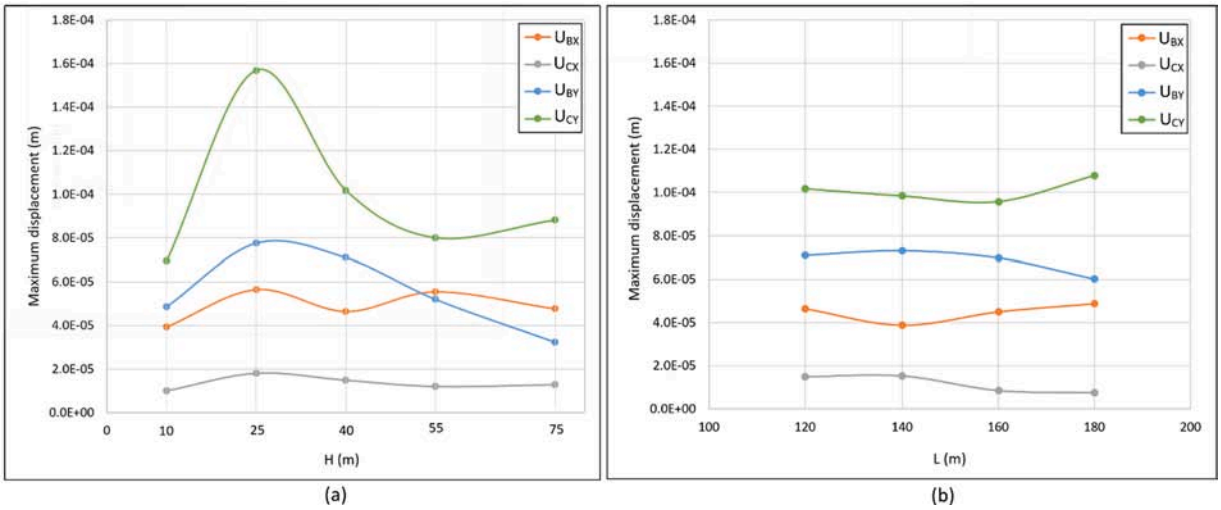

Fig. 10. Maximum displacement results under different heights and widths of soil model.

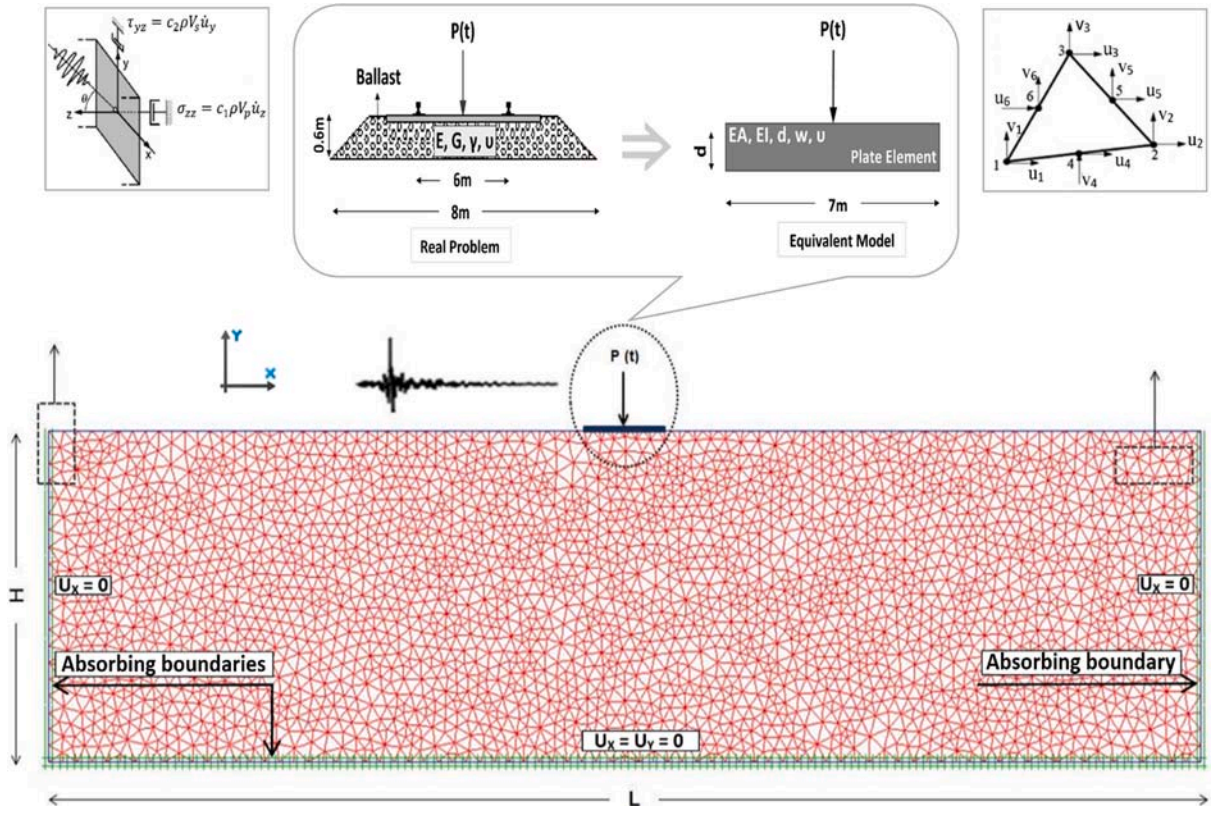

Fig. 11. Typical 2D FE model of the track-ground system developed in Plaxis.

of stiffness on system damping. Standard settings were chosen for the numerical analysis. The standard and default settings in Plaxis assume no Rayleigh damping (alpha and beta are equal to zero).

The numerical FE model in this study to simulate the load of a passing train assumes that the applied load acts with a constant velocity on an infinite beam resting on a homogeneous elastic half-space. As most of the damping is produced by the propagation of a radioactive wave (geometric damping), the Rayleigh damping can be appropriately reduced in the point vibration source problem. In single-source problems, radiation or geometric damping is the most significant contributor to the system damping. In this type of problem, it may not be necessary to include Rayleigh damping because most of the damping is caused by a radial spread of waves (geometric damping) (Plaxis 2D-Version 8 User Guide, 2002). As the wave spreads around and beneath the soil, radiation damping significantly attenuates the vibration, which is why we consider it in this study. Moreover, several field studies have been conducted on the shear strain in clay and sandy soils to study the variation in material damping. Experimental results show a small damping (near zero) in the soil environments with extremely low deformations (Bolton Seed et al., 1986; Vucetic et al., 1991). The in-situ measurements show that the vibration amplitudes in the surrounding soil under cycling loading generated by the passage of HSTs are not large enough to cause remarkable deformations. Therefore, material damping was not considered in the present study.

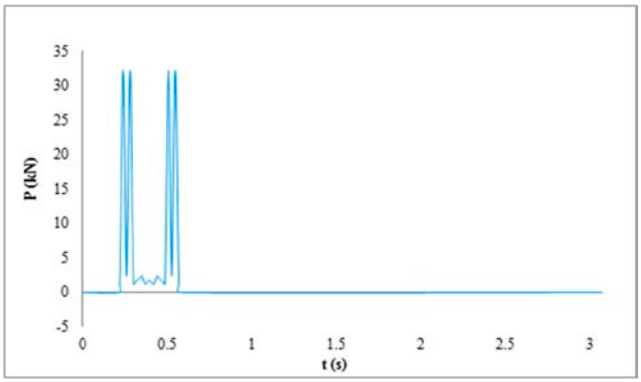

Fig. 12. Time-dependent variation of the influence forces for HST passage (Göktepe, 2013).

In the present study, the high-speed railway line passes through the Kirkpinar-Sapanca village, which has an alluvial soil medium with low shear strength and bearing capacity ($V_S = 200$ m/s). Owing to this low bearing capacity, strengthening the weak subgrade soil layer under the existing tracks is necessary to increase the track-ground stiffness and reduce the differential settlement during the passage of trains. Therefore, the subgrade soil strength properties of the experimental site under the track bed were improved using suitable geotechnical methods. Consequent to this improvement, the soil medium became more rigid, and the deformations occurring during the passage of HSTs remained in the elastic zone. Thus, a linear elastic soil model was used due to the small deformations induced by a dynamic wave.

The distribution of the HST load on the slab track was accurately simulated as a dynamic point load, which represents a single wheel load (90 kN) corresponding to the railway engine HT65000 passing with a velocity of 250 km/h for a forcing amplitude of 32.5 kN (Fig. 12). The numerical analysis assumes that the applied moving load acts with a constant velocity on an infinite beam resting on a homogeneous elastic surface. The standard railway superstructure is modeled as a beam element with the required moment of inertia and moment of area. The rigidity of the beam element is considered to be approximately equivalent to the rigidity of the railway track components (rail, sleepers, and ballast), which reflects the mechanical behavior of the superstructure under train loading (Estorff et al., 2003; Göktepe, 2013). This proposed simplified superstructure was considered for model verification.

During the HST movement, wave propagation occurs both in

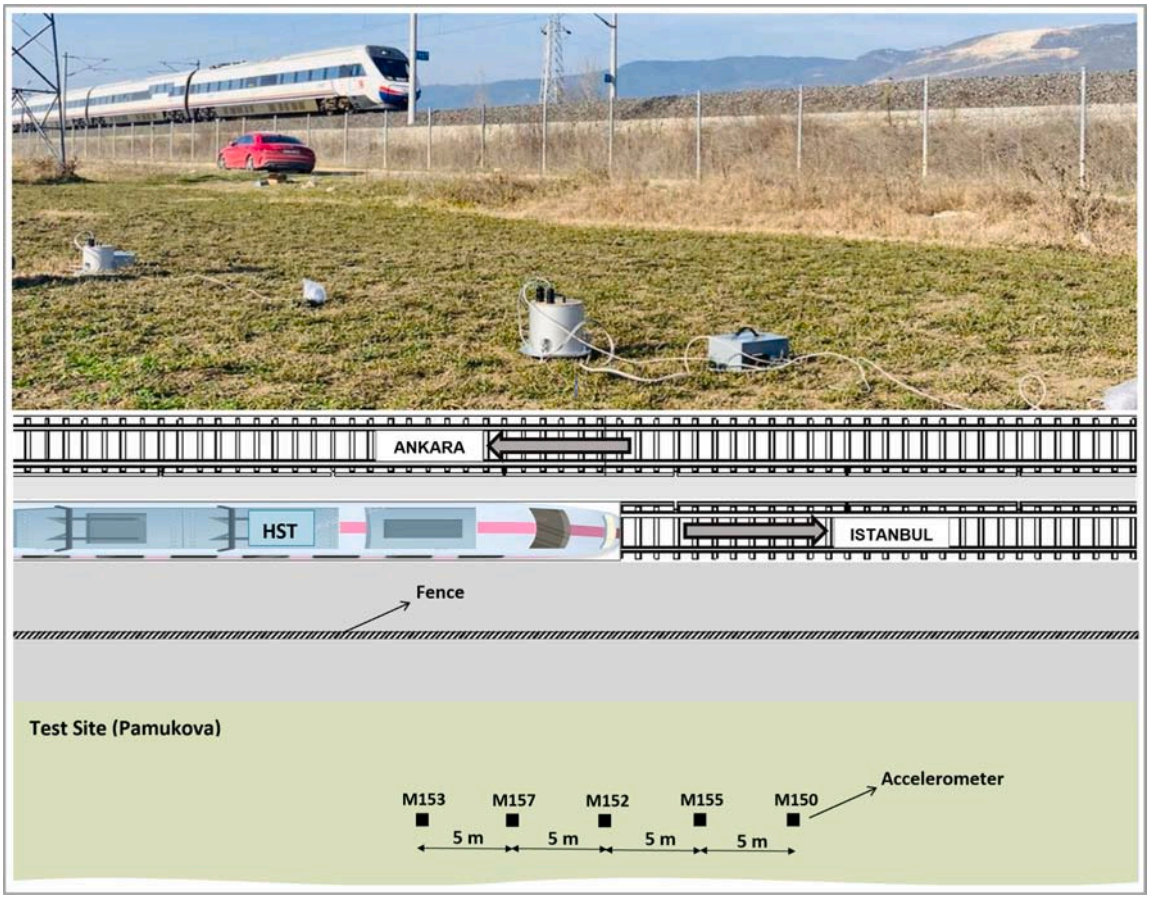

Fig. 13. Measurement site of ground vibration on the Istanbul-Ankara high-speed railway.

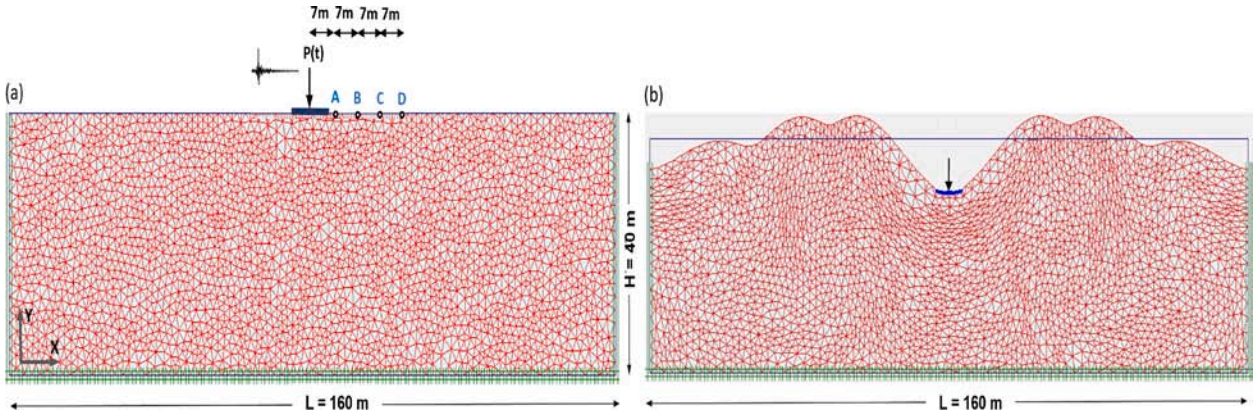

Fig. 14. (a) The FE model (before calculation) and (b) deformed mesh (after calculation).

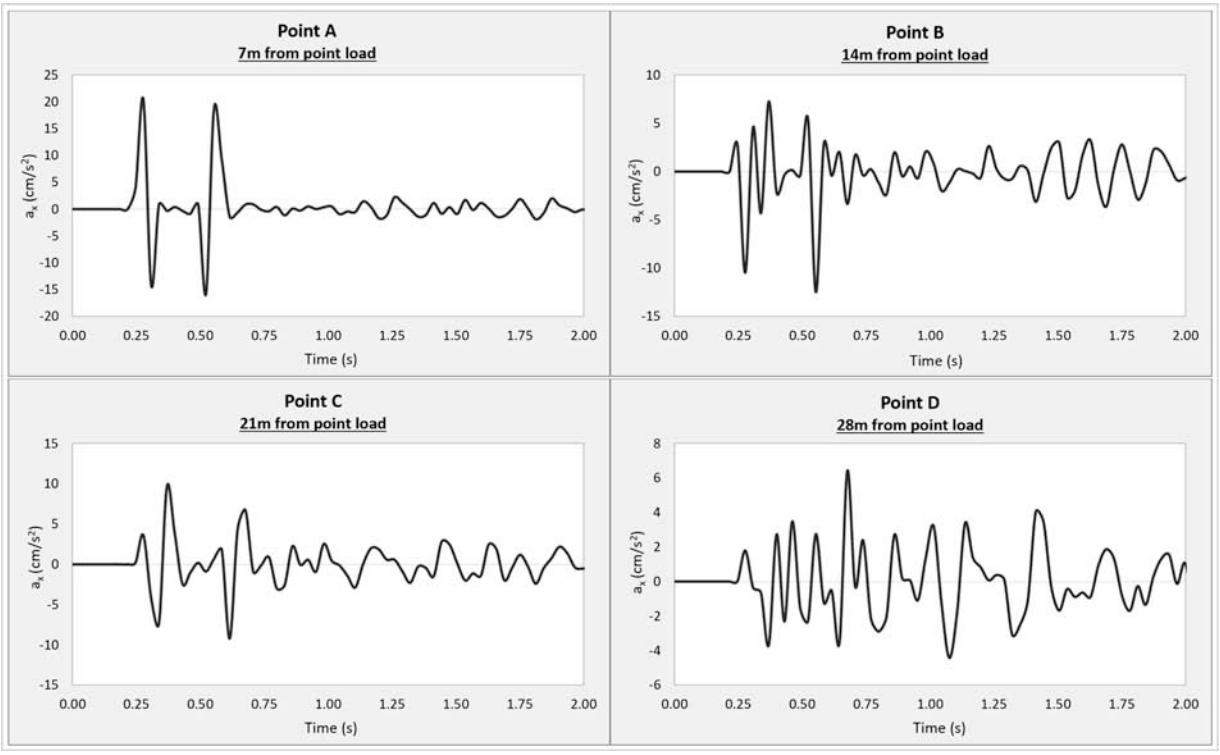

Fig. 15. The time history of the horizontal acceleration at selected points at different distances from the point load.

longitudinal and perpendicular directions to the track line. However, since the vibration waves propagating along the track line spread along the railway platform axis, the surrounding structures are more affected by the vibrations radiating perpendicular to the track line. The authors performed a field experiment on the Istanbul-Ankara high-speed railway at Pamukova-Turkey to observe the vibration effect of HST in both longitudinal and perpendicular directions to the track line. Based on the measured data, it was proved that the train-induced ground-born vibration in the longitudinal direction can be omitted when compared to the wave propagation perpendicular to the track line (Fig. 13). In light of this observation, a 2D model was established and the HST effects were defined as a point load to consider a wave propagation perpendicular to the railway track.

4.3. Numerical analysis and model validation

The numerical analysis of the proposed track-ground coupled model for different points was performed in the time domain under plain-strain conditions using the Plaxis FE package. In this study, the relative horizontal and vertical accelerations of points A, B, C, and D were determined using 2D linear elastic analysis, as shown in Figs. 15 and 16. The PGAs of the FE analysis for different points are listed in Table 3.

Figs. 15 and 16 shows the horizontal and vertical accelerations (a_x and a_y) for the selected points (see Fig. 14 (a)) at distances of x = 7 m, 14 m, 21 m, and 28 m from the load axis. Acceleration amplitudes were significantly decreased with distance from the dynamic load, as expected. The highest acceleration is observed at checkpoint A, which is located near the load axis. The checkpoints B, C, and D have smaller accelerations as the distance increases along the × direction. We also observed that the largest peak accelerations are related to the vibration calculated in the vertical direction whereas the smallest peak accelerations occur in the horizontal direction, as shown in Table 3.

The validation of the present numerical model was performed using field measurement data, which the authors have presented in the previous section. The measured and computed results were compared for the validation using PGA values. Fig. 17 shows a comparison between

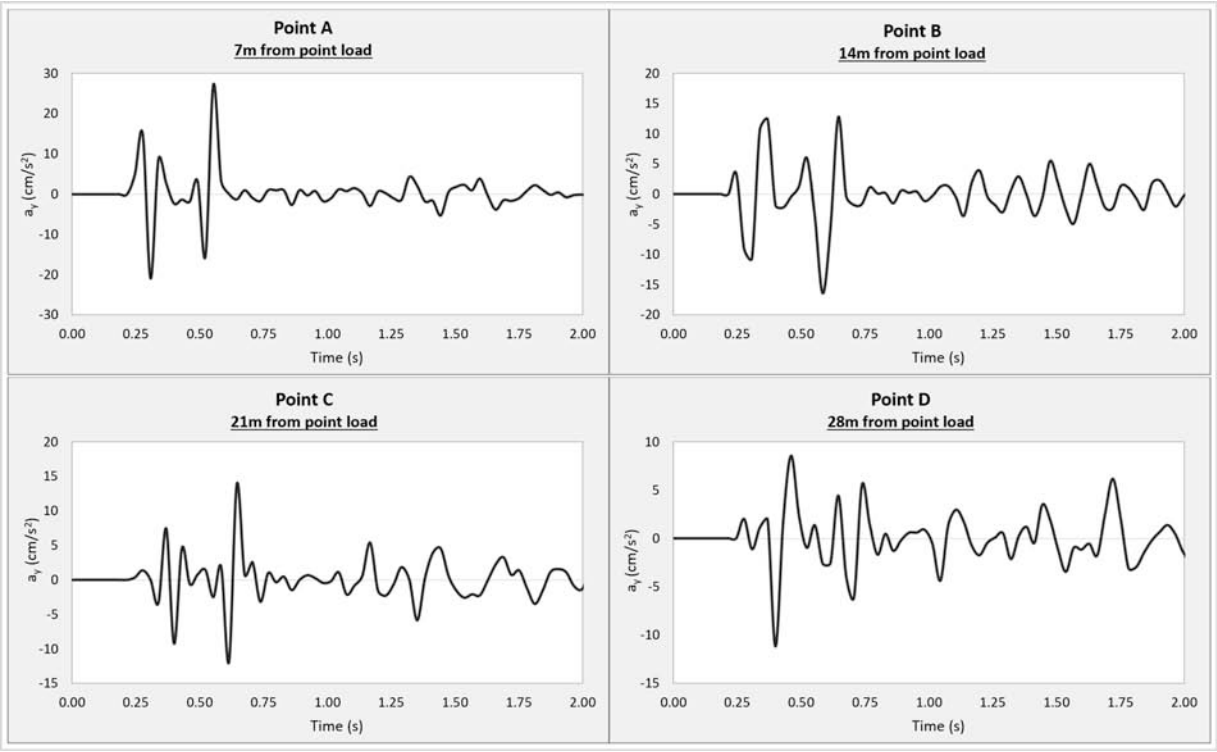

Fig. 16. The time history of the vertical acceleration at selected points at different distances from the point load.

Table 3
PGA values in horizontal and vertical directions (cm/s^2).

Points	Distance from point load (m)	FEM	
		a_x	a_y
A	7	20.40	27.20
B	14	12.50	16.40
C	21	9.60	13.80
D	28	6.40	11.20

the measured and calculated PGAs on the ground at distances of 7, 14, 21, and 28 m from the track; a reasonable agreement can be observed between them (Fig. 16). The vertical and horizontal PGAs for the selected points are presented and summarized in Table 4. A good agreement can be observed between the measured and calculated accelerations on the ground. The compatibility of the results proves that the verified FE model can be applied to vibration analysis.

4.4. Parametric study on the impact of soil conditions

In this study, the railway track soil classification is based on the shear wave velocity, Vs_{30}, which is employed as the key categorization parameter in modern seismic codes from a structural engineering perspective. According to the Turkish Building Earthquake Code 2018 (TBEC 2018), rock and soil can be divided into six categories: hard rock, rock, dense soil, medium-hard soil, soft soil, and special soils requiring site-specific evaluation. The corresponding shear wave velocity (V_S) ranges for these soils are listed in Table 5.

To investigate the effect of soil properties on the train-induced vibrations, four types of soils were analyzed: hard rock, dense soil, medium-hard soil and soft soil. In the present study, a 2D linear elastic analysis was performed and the relative horizontal and vertical accelerations at the selected points (see Fig. 13(a)) were compared and shown graphically. The mechanical properties of different soil types are shown in Table 6.

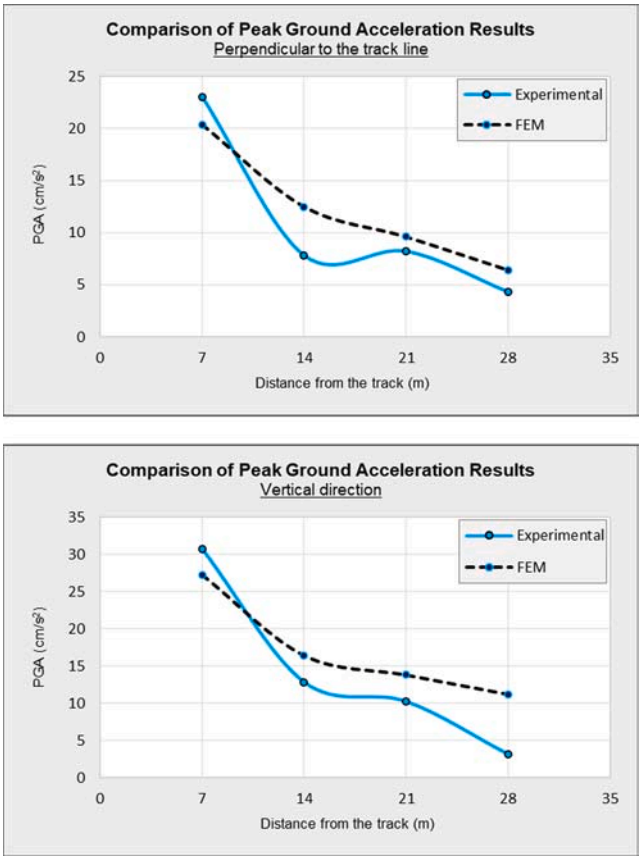

Fig. 17. Comparison of measured and calculated peak ground accelerations.

Table 4
Comparing PGA of the measured and calculated accelerations (cm/s^2).

Device/measuring point	Distance from track (m)	Experimental		FEM	
		$a_{(N-S)}$	$a_{(U-D)}$	a_x	a_y
M168 / A	7	23.00	30.70	20.40	27.20
M166 / B	14	7.80	12.80	12.50	16.40
M171 / C	21	8.20	10.20	9.60	13.80
M150 / D	28	4.30	3.10	6.40	11.20

Table 5
Rock and soil classifications according to the TBEC 2018.

Soil Class	Soil Types	Average Shear Wave Velocity V_S (m/s)
ZA	Hard rock	> 1500
ZB	Rock	760–1500
ZC	Dense soil	360–760
ZD	Medium-hard soil	180–360
ZE	Soft soil	<180
ZF	Special soils requiring special evaluation	–

Table 6
Mechanical properties of different soil types (Karahan, 2012).

Parameters	Hard rock	Dense soil	Medium-hard soil	Soft soil
γ (kN/m^3)	26.50	21.64	18.64	16.67
E (kN/m^2)	4.5×10^7	3.01×10^6	3.61×10^5	3.45×10^4
υ (-)	0.125	0.35	0.30	0.25
V_S (m/s)	2720	710	270	100

Based on the established FE model and numerical analysis, the time histories and the vertical and horizontal PGAs on the ground at selected points are calculated and shown in Figs. 18 and 19, respectively. The extracted PGAs are given in Table 7.

Comparing the maximum accelerations at the nearest and furthest points to the track (A and D), we find that the maximum horizontal acceleration values for point A on soft soil are respectively 56%, 88%, and 98% higher than medium, dense and hard rock soils. Moreover, the maximum horizontal acceleration values for point D on soft soil are respectively 31%, 55%, and 89% higher than medium, dense, and hard rock soils. When considering the results in the vertical direction, the maximum acceleration values for point A on soft soil are respectively 25%, 76%, and 92% higher than medium, dense, and hard rock soils. Furthermore, the vertical PGA values for point D on soft soil are 33%, 78%, and 89% higher than medium, dense, and hard rock, respectively.

The computational results for different soil conditions in the horizontal and vertical directions, as shown in Fig. 19(a) and (b), also show that the PGA diminishes by almost 58% from point A to point D in the soft soil condition in the horizontal direction and 36% in the vertical direction; this difference is 25% and 44%, respectively, in medium soil conditions. The attenuation in a dense soil condition is extremely low, and almost no attenuation was noticed in the hard rock site condition.

5. Conclusions

An in-situ test for ground vibration due to the passage of an HST (HT65000) at a speed of 250 km/h was performed on the Istanbul-Ankara high-speed railway in Turkey. During the test, the resulting time histories of the vertical and horizontal accelerations on the ground were obtained. Further, a numerical prediction model for train-induced ground vibrations was developed and validated with in-situ measurements. In this study, a 2D linear elastic analysis was performed using the Plaxis FE package. The horizontal and vertical accelerations at the selected points were obtained and represented graphically. A linear elastic soil model was used due to the small deformations induced by dynamic waves. The HST effects were defined as a point load for wave propagation in a direction perpendicular to the railway track. The numerical FE model simulated the passing train load by assuming that the applied moving load acts with a constant velocity on an infinite beam resting on a homogeneous elastic surface. Finally, to investigate the effect of soil properties on train-induced vibrations, an analysis was performed on four soil types with different rigidities using the verified model. The relative horizontal and vertical accelerations for different soil conditions were obtained for a comparison.

The study's field and numerical results reveal the following:

(1) The PGA results in both directions show that the vertical component of train-induced vibrations has a greater impact than the horizontal component in the near-field ground surface.
(2) Ground-borne vibration characteristics in the downward and perpendicular directions during the passage of the HST are different. Accordingly, vibration measurements should be performed in all directions.
(3) Underlying soil stiffness affect environmental ground vibration generation and propagation because of HST traffic. The PGA values increase from hard rock to soft soil.
(4) The dynamic analysis under different soil conditions showed that the vibration levels in both directions decreased with distance from the track. However, it should be noted that it is not possible for numerical models to capture vibration amplification regions because of the heterogeneous distribution of soil components. In such complex soil formations, it is difficult to incorporate the wave interference problem into a numerical model.
(5) By comparing the measured and calculated PGAs, we see that the numerical results are in good agreement with the experimental results. This compatibility of the results proves that the verified FE model can be applied to the analysis of vibrations.
(6) The applied FE model can be considered as a useful prediction tool and easily implemented by engineers not accustomed to handling complex numerical models. The simplification of the proposed numerical model can provide valuable guidelines for researchers as well as railway and vibration engineers to study the effect of ground-borne vibrations in a fast and effective way.

Simplified computational models validated by the test results in full-scale field conditions may help researchers determine further investigation strategies to develop cost-effective mitigation measures for structures with sensitive devices near the railway track and significantly contribute to understanding complex wave propagation problems. In addition to the accuracy of the proposed numerical model for the ground-borne wave propagation problem, the acceptable computational time and memory requirements in the implemented FE analysis are considered as important governing parameters.

Vibration measurement data collected from parametric experiments with a simple numerical model for various soil characteristics can guide structural engineers and city planners during the feasibility study of a project. This data can be particularly useful when planning residential and industrial facilities at new locations near railroads, to avoid the adverse effects of environmental vibrations caused by HSTs.

Declaration of Competing Interest

The authors declare the following financial interests/personal relationships which may be considered as potential competing interests: Erkan CELEBI reports financial support was provided by TUBITAK (The Scientific and Technological Research Council of Turkey). Osman KIRTEL reports a relationship with Sakarya University of Applied Science that includes: employment. Erkan CELEBI reports a relationship with Sakarya University that includes: employment. Abdullah Can ZULFIKAR reports a relationship with Gebze Technical University that includes:

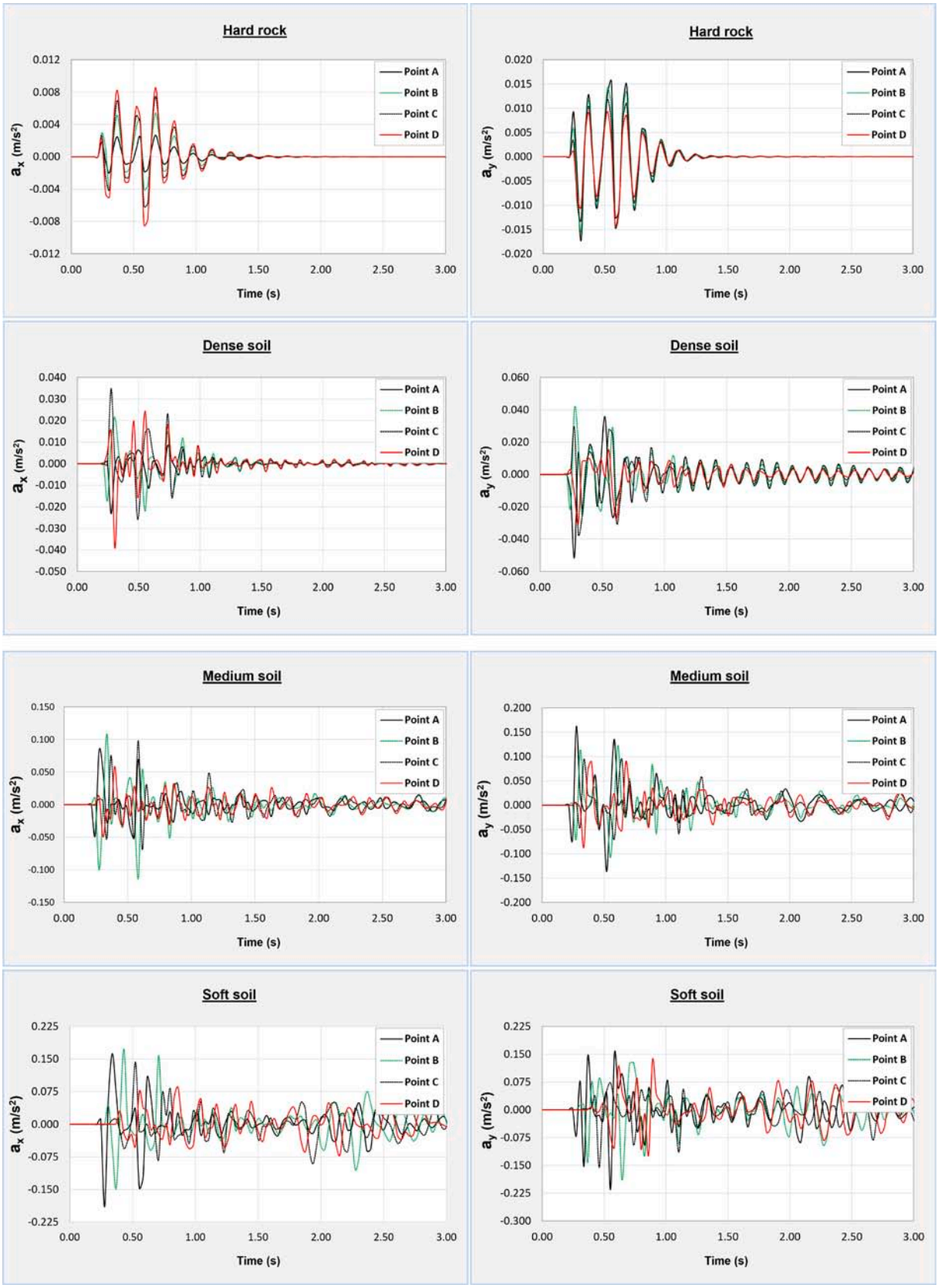

Fig. 18. The time history of the horizontal and vertical accelerations at selected points for different soil types.

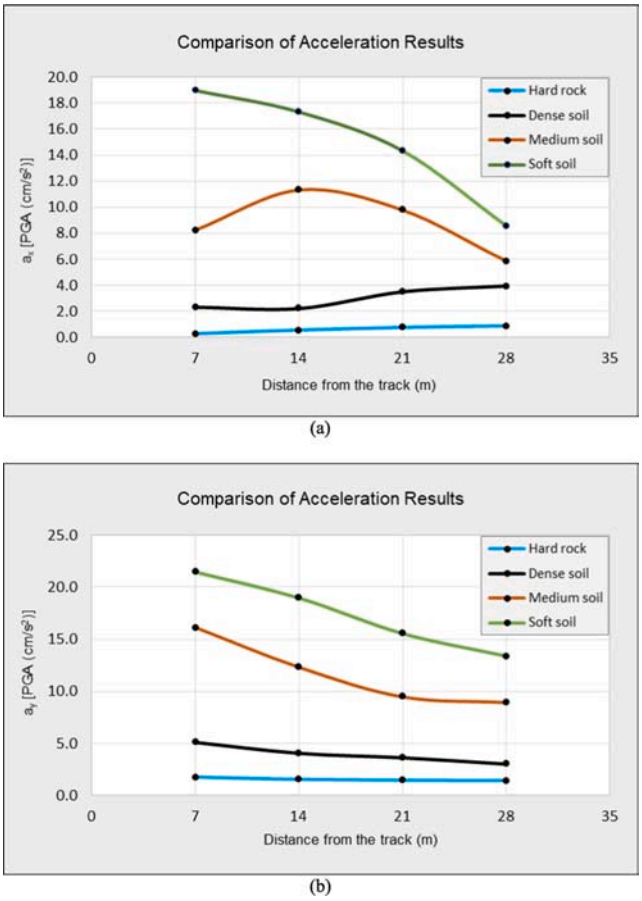

Fig. 19. Comparison of calculated peak ground accelerations for different soil types (a) in horizontal direction and (b) in vertical direction.

Table 7
Summary of maximum vibration accelerations at different points.

Soil Types	a_x (cm/s^2)				a_y (cm/s^2)			
	A	B	C	D	A	B	C	D
Hard rock	0.30	0.50	0.70	0.90	1.70	1.50	1.40	1.40
Dense soil	2.30	2.20	3.50	3.90	5.10	4.10	3.70	3.00
Medium soil	8.20	11.30	9.80	5.90	16.10	12.30	9.50	9.00
Soft soil	19.00	17.30	14.30	8.60	21.50	19.00	15.60	13.40

employment. Fatih GOKTEPE reports a relationship with Bartin University that includes: employment.

Acknowledgements

This research is funded by the TÜBİTAK (The Scientific and Technological Research Council of Turkey) under the grant No: 217M427. Their financial support is gratefully acknowledged.

References

Andersen, L., Jones, C.J.C., 2006. Coupled boundary and finite element analysis of vibration from railway tunnels—a comparison of two- and three-dimensional models. J. Sound Vib. 293 (3), 611–625. https://doi.org/10.1016/j.jsv.2005.08.044.

Auersch, L., 2005. The excitation of ground vibration by rail traffic: theory of vehicle–track–soil interaction and measurements on high-speed lines. J. Sound Vib. 284 (1), 103–132. https://doi.org/10.1016/j.jsv.2004.06.017.

Auersch, L., 1994. Wave propagation in layered soil dynamics: Theoretical solution in wave number domain and experimental results of hammer and railway traffic excitation. J. Sound Vib. 173 (2), 233–264. https://doi.org/10.1006/jsvi.1994.1228.

Basack, S., Indraratna, B., Rujikiatkamjorn, C., 2016. Modeling the performance of stone column–reinforced soft ground under static and cyclic loads. J. Geotech. Geoenv. Eng. 142 (2), 04015067. https://doi.org/10.1061/(ASCE)GT.1943-5606.0001378.

Brinkgreve, R.B.J., Al-Khoury, R., Bakker, K.J., Bonnier, P.G., Brand, P.J.W., Broere, W., Burd, H.J., Soltys, G., Vermeer, P.A., Haag, D.D., 2002. Plaxis finite element code for soil and rock analyses. Published and distributed by A.A Balkema Publisher, The Netherlands.

Çelebi, E., Fırat, S., Beyhan, G., Çankaya, İ., Vural, İ., Kırtel, O., 2009. Field experiments on wave propagation and vibration isolation by using wave barriers. Soil Dyn. Earthq. Eng. 29 (5), 824–833. https://doi.org/10.1016/j.soildyn.2008.08.007.

Çelebi, E., Kırtel, O., 2013. Non-linear 2-D FE modeling for prediction of screening performance of thin-walled trench barriers in mitigation of train-induced ground vibrations. Constr. Build. Mater. 42, 122–131. https://doi.org/10.1016/j.conbuildmat.2012.12.071.

Celebi, E., 2006. Three-dimensional modelling of train-track and sub-soil analysis for surface vibrations due to moving loads. Appl. Math. Comput. 179 (1), 209–230. https://doi.org/10.1016/j.amc.2005.11.095.

Chen, Q., Li, Y., Ke, W., Basack, S., Xu, C., 2021. "New Technique for Ground Vibration Mitigation by Horizontally Buried Hollow Pipes", ASCE Library. Int. J. Geomech. 21 (7) https://doi.org/10.1061/(ASCE)GM.1943-5622.0002077.

Connolly, D., Giannopoulos, A., Forde, M.C., 2013. Numerical modelling of ground borne vibrations from high speed rail lines on embankments. Soil Dyn Earthq Eng. 46, 13–19. https://doi.org/10.1016/j.soildyn.2012.12.003.

Costa, P.A., Calçada, R., Cardoso, A.S., 2012. Influence of train dynamic modelling strategy on the prediction of track–ground vibrations induced by railway traffic. In:

Proc Inst Mech Eng, Part F: J Rail Rapid Transit 226(4), 434-450, https://doi.org/10.1177%2F0954409711433686.
Degrande, G., Schillemans, L., 2001. Free Field Vibrations During the Passage of a Thalys High-Speed Train at Variable Speed. J. Sound Vib. 247 (1), 131–144. https://doi.org/10.1006/jsvi.2001.3718.
Faizan, A.A., Kırtel, O., 2017. Dynamic behaviour of railway bridge subjected to different strong ground motions considering soil-structure interaction. In: International Conference on Research in Education and Science, Ephesus - Kusadasi, Turkey: ICRES, pp. 641-647.
Faizan, A.A., 2017. Seismic analysis of railway bridges considering soil-structure interaction. Master thesis. Sakarya University, Institute of Natural Sciences, Sakarya, Turkey.
Forrest, J.A., Hunt, H.E.M., 2006. A three-dimensional tunnel model for calculation of train-induced ground vibration. J. Sound Vib. 294 (4), 678–705. https://doi.org/10.1016/j.jsv.2005.12.032.
François, S., Lombaert, G., Degrande, G., 2005. Local and global shape functions in a boundary element formulation for the calculation of traffic induced vibrations. Soil Dyn. Earthq. Eng. 25 (11), 839–856. https://doi.org/10.1016/j.soildyn.2005.05.002.
Galavi, V., Brinkgreve, R., 2014. In: Numerical Methods in Geotechnical Engineering. CRC Press, pp. 235–240. https://doi.org/10.1201/b17017-44.
Galvín, P., Domínguez, J., 2009. Experimental and numerical analyses of vibrations induced by high-speed trains on the Córdoba-Málaga line. Soil Dyn. Earthq. Eng. 29 (4), 641–657. https://doi.org/10.1016/j.soildyn.2008.07.001.
Galvín, P., Romero, A., Domínguez, J., 2010. Fully three-dimensional analysis of high-speed train–track–soil-structure dynamic interaction. J. Sound Vib. 329 (24), 5147–5163. https://doi.org/10.1016/j.jsv.2010.06.016.
Galvín, P., Romero, A., 2014. A 3D time domain numerical model based on half-space Green's function for soil–structure interaction analysis. Comput. Mech. 53 (5), 1073–1085. https://doi.org/10.1007/s00466-019-01720-4.
Göktepe, F., 2013. The parametric performance investigation of the barrier systems for the prevention of the induced vibrations due to high speed trains in the nearby structures. PhD thesis. Sakarya University, Institute of Natural Sciences, Sakarya, Turkey.
Gupta, S., Degrande, G., Lombaert, G., 2009. Experimental validation of a numerical model for subway induced vibrations. J. Sound Vib. 321, 786–812. https://doi.org/10.1007/978-3-540-74893-9_15.
Gupta, S., Liu, W., Degrande, G., Lombaert, G., Liu, W., 2008. Prediction of vibrations induced by underground railway traffic in Beijing. J. Sound Vib. 310 (3), 608–630. https://doi.org/10.1016/j.jsv.2007.07.016.
Seed, H.B., Wong, R.T., Idriss, I.M., Tokimatsu, K., 1986. Moduli and damping factors for dynamic analyses of cohesionless soils. J. Geotech. Eng. 112 (11), 1016–1032. https://doi.org/10.1061/(ASCE)0733-9410(1986)112:11(1016).
Karahan, N., 2012. The effects of the soil conditions on the structural response. Master thesis. Sakarya University, Institute of Natural Sciences, Sakarya, Turkey.
Kogut, J., Degrande, G., Haegeman, W., 2003. Free field vibrations due to the passage of an IC train and a Thalys HST on the high speed track L2 Brussels-Köln. 6th National Congress on Theoretical and Applied Mechanics.
Komazawa, M., Morikawa, H., Nakamura, K., Akamatsu, J., Nishimura, K., Sawada, S., Erken, A., Onalp, A., 2002. Bedrock structure in Adapazari, Turkey—a possible cause of severe damage by the 1999 Kocaeli earthquake. Soil Dyn. Earthq. Eng. 22 (9–12), 829–836. https://doi.org/10.1016/S0267-7261(02)00105-7.
Kontoni, D.P.N., Farghaly, A.A., 2020. Mitigation of train-induced vibrations onnearby high-rise buildings by open or geofoam-filled trenches. J. Vibroengineering 22 (2), 416–426. https://doi.org/10.21595/jve.2019.20523.
Kouroussis, G., Verlinden, O., 2013. Prediction of railway induced ground vibration through multibody and finite element modelling. Mech. Sci. 4 (1), 167–183. https://doi.org/10.5194/ms-4-167-2013.
Kumar, A., Choudhury, M., 2018. Development of new prediction model for capacity of combined pile-raft foundations. Comput. Geotech. 97, 62–68. https://doi.org/10.1016/j.compgeo.2017.12.008.
Kumar, A., Patil, M., Choudhury, M., 2017. Soil-structure interaction in a combined pile-raft foundation: A case study. Proc. Inst. Civ. Eng. Geotech. Eng. 170 (2), 117–128. https://doi.org/10.1680/jgeen.16.00075.
Liao, W.I., Teng, T.J., Yeh, C.S., 2005. A method for the response of an elastic half-space to moving sub-Rayleigh point loads. J. Sound Vib. 284 (1), 173–188. https://doi.org/10.1016/j.jsv.2004.06.005.
Lombaert, G., Degrande, G., Kogut, J., François, S., 2006. The experimental validation of a numerical model for the prediction of railway induced vibrations. J. Sound Vib. 297 (3), 512–535. https://doi.org/10.1016/j.jsv.2006.03.048.
Lombaert, G., Degrande, G., 2001. Experimental validation of a numerical prediction model for free field traffic induced vibrations by in situ experiments. Soil Dyn Earthq Eng. 21 (6), 485–497. https://doi.org/10.1016/S0267-7261(01)00017-3.
Lombaert, G., Degrande, G., 2009. Ground-borne vibration due to static and dynamic axle loads of InterCity and high-speed trains. J. Sound Vib. 319 (3), 1036–1066. https://doi.org/10.1016/j.jsv.2008.07.003.
Lysmer, J., Kuhlemeyer, R.L., 1969. "Finite dynamic model for infinite media. ASCE J. Eng. Mech. 95 (4), 859–877. https://doi.org/10.1061/JMCEA3.0001144.
Metrikine, A.V., Vrouwenvelder, A.C.W.M., 2000. Surface ground vibration due to a moving train in a tunnel: Two-dimensional model. J. Sound Vib. 234 (1), 43–66. https://doi.org/10.1006/jsvi.1999.2853.
Vucetic, M., Associate Member, A.S.C.E., Dobry, R., Member, A.S.C.E., 1991. Effect of Soil Plasticity on Cyclic Response. J. Geotech. Eng. 117.
von Estorff, O., Firuziaan, M., Friedrich, K., Pflanz, G., Schmid, G.,2002. A three-dimensional FEM/BEM model for the investigation of railway tracks. In: Wave 2002. Wave propagation – Moving load – Vibration reduction (Eds.: N. Chouw, G. Schmid). Swets & Zeitlinger, Lisse, 2003. pp. 157–171.
Plaxis 2D-Version 8 User Guide, Plaxis Finite Element Code for Soil and Rock Analyses, Edited by Brinkgreve, R B. J., Delft University of Technology & Plaxis b.v., The Netherlands, A.A. Balkema Publishers, 2002.
Rosset, J.M., Kausel, F., 1976. Dynamic soil-structure interaction. In: Second International Conference on Numerical Methods in Geomechanics, Virginia, USA, pp. 3–19.
Sheng, X., Jones, C.J.C., Petyt, M., 1999. Ground vibration generated by a load moving along a railway track. J. Sound Vib. 228 (1), 129–156. https://doi.org/10.1006/jsvi.1999.2406.
Sheng, X., Jones, C.J.C., Thompson, D.J., 2005. Responses of infinite periodic structures to moving or stationary harmonic loads. J. Sound Vib. 282 (1), 125–149. https://doi.org/10.1016/j.jsv.2004.02.050.
Takemiya, H., 2003. Simulation of track–ground vibrations due to a high-speed train: the case of X-2000 at Ledsgard. J. Sound Vib. 261 (3), 503–526. https://doi.org/10.1016/S0022-460X(02)01007-6.
TCDD National High-Speed Train Project. The State Railways of the Republic of Turkey (TCDD), http://www.tcdd.gov.tr/; 2017.
Thompson, D.J., Jiang, J., Toward, M.G.R., Hussein, M.F.M., Ntotsios, E., Dijckmans, A., Coulier, P., Lombaert, G., Degrande, G., 2016. Reducing railway-induced ground-borne vibration by using open trenches and soft-filled barriers. Soil Dyn. Earthq. Eng. 88, 45–59. https://doi.org/10.1016/j.soildyn.2016.05.009.
Triepaischajonsak, N., Thompson, D.J., 2015. A hybrid modelling approach for predicting ground vibration from trains. J. Sound Vib. 335, 147–173. https://doi.org/10.1016/j.jsv.2014.09.029.
Turkish Building Earthquake Code (TBEC), 2018.
Wanming, Z., Zhenxing, H., Xiaolin, S., 2010. Prediction of highspeed train induced ground vibration based on train-track-ground system model. Earthquake Eng. Eng. Vibr.. 9 (4), 545–554. https://doi.org/10.1007/s11803-010-0036-y.
Xia, H., Chen, J., Wei, P., Xia, C., Roeck, G.D., Degrande, G., 2009. Experimental investigation of railway train-induced vibrations of surrounding ground and a nearby multi-story building. Earthquake Eng. Eng. Vibr. 8 (1), 137–148. https://doi.org/10.1007/s11803-009-8101-0.
Yang, Y.B., Hung, H.H., Chang, D.W., 2003. Train-induced wave propagation in layered soils using finite/infinite element simulation. Soil Dyn. Earthq. Eng. 23 (4), 263–278. https://doi.org/10.1016/S0267-7261(03)00003-4.
Yaseri, A., Bazyar, M.H., Hataf, N., 2014. 3D coupled scaled boundary finite-element/finite-element analysis of ground vibrations induced by underground train movement. Comput. Geotech. 60, 1–8. https://doi.org/10.1016/j.compgeo.2014.03.013.
Zhang, L., Feng, Q., 2011. In: Experimental analysis on ground vibration generated by high-speed train. ASCE, Chengdu, China, pp. 1597–1602.
Zou, C., Wang, Y., Tao, Z., 2020. Train-Induced Building Vibration and RadiatedNoise by Considering Soil Properties. Sustainability 12 (3), 1–17. https://doi.org/10.3390/su12030937.